




RESEARCH ARTICLE

Joint-label fusion brain atlases for dementia research in Down syndrome

Nazek Queder^{1,2}  | Michael J. Phelan³ | Lisa Taylor¹ | Nicholas Tustison⁴ | Eric Doran⁵ | Christy Hom¹ | Dana Nguyen¹ | Florence Lai⁶ | Margaret Pulsifer⁶ | Julie Price⁶ | William C. Kreisl⁷ | Herminia D. Rosas⁶ | Sharon Krinsky-McHale⁸ | Adam M. Brickman^{7,9} | Michael A. Yassa^{1,2,11}  | Nicole Schupf^{7,9} | Wayne Silverman⁵ | Ira T. Lott⁵ | Elizabeth Head¹⁰ | Mark Mapstone¹¹ | David B. Keator¹  | for the Alzheimer's Biomarkers Consortium[†]

¹Department of Psychiatry and Human Behavior, University of California Irvine, Irvine, California, USA

²Department of Neurobiology and Behavior and Center for the Neurobiology of Learning and Memory, University of California Irvine, Irvine, California, USA

³Institute for Memory Impairments and Neurological Disorders, University of California Irvine, Irvine, California, USA

⁴Department of Radiology, University of Virginia, Charlottesville, Virginia, USA

⁵Department of Pediatrics, University of California, Irvine Medical Center, Orange, California, USA

⁶Massachusetts General Hospital, Harvard University, Boston, Massachusetts, USA

⁷Department of Neurology, Columbia University, New York, New York, USA

⁸New York State Institute for Basic Research in Developmental Disabilities, New York, New York, USA

⁹Taub Institute for Research on Alzheimer's Disease and the Aging Brain, Department of Neurology, Vagelos College of Physicians and Surgeons, Columbia University, New York, New York, USA

¹⁰Department of Pathology & Laboratory Medicine, University of California Irvine, Irvine, California, USA

Abstract

Research suggests a link between Alzheimer's Disease in Down Syndrome (DS) and the overproduction of amyloid plaques. Using Positron Emission Tomography (PET) we can assess the in-vivo regional amyloid load using several available ligands. To measure amyloid distributions in specific brain regions, a brain atlas is used. A popular method of creating a brain atlas is to segment a participant's structural Magnetic Resonance Imaging (MRI) scan. Acquiring an MRI is often challenging in intellectually-impaired populations because of contraindications or data exclusion due to significant motion artifacts or incomplete sequences related to general discomfort. When an MRI cannot be acquired, it is typically replaced with a standardized brain atlas derived from neurotypical populations (i.e. healthy individuals without DS) which may be inappropriate for use in DS. In this project, we create a series of disease and diagnosis-specific (cognitively stable (CS-DS), mild cognitive impairment (MCI-DS), and dementia (DEM-DS)) probabilistic group atlases of participants with DS and evaluate their accuracy of quantifying regional amyloid load compared to the individually-based MRI segmentations. Further, we compare the diagnostic-specific atlases with a probabilistic atlas constructed from similar-aged cognitively-stable neurotypical participants. We hypothesized that regional PET signals will best match the individually-based MRI segmentations by using DS group atlases that aligns with a participant's disorder and disease status (e.g. DS and MCI-DS). Our results vary by brain region but generally show that using a disorder-specific atlas in DS better matches the individually-based MRI segmentations than using an atlas constructed

[†]Alzheimer's Biomarker Consortium–Down Syndrome (ABC-DS) Investigators

This is an open access article under the terms of the [Creative Commons Attribution-NonCommercial](https://creativecommons.org/licenses/by-nc/4.0/) License, which permits use, distribution and reproduction in any medium, provided the original work is properly cited and is not used for commercial purposes.

© 2022 The Authors. *Alzheimer's & Dementia: Diagnosis, Assessment & Disease Monitoring* published by Wiley Periodicals, LLC on behalf of Alzheimer's Association

¹¹Department of Neurology, University of California Irvine, Irvine, California, USA

Correspondence

Nazek Queder, University of California, Irvine Hall rm. 164 – Zot 3960, Irvine, CA 92697, USA.
E-mail: nqueder@uci.edu

Funding information

National Institute on Aging, Grant/Award Numbers: U01AG051412-01, R01AG053555; Eunice Kennedy Shriver National Institute of Child Health and Human Development; The Alzheimer's Disease Research Centers Program, Grant/Award Numbers: P50 AG008702, P30 AG062421, P50 AG16537, P50 AG005133, P50 AG005681, P30 AG062715; Eunice Kennedy Shriver Intellectual and Developmental Disabilities Research Centers Program, Grant/Award Numbers: U54 HD090256, U54 HD087011; National Centers for Advancing Translational Sciences, Grant/Award Numbers: UL1 TR001873, UL1 TR002373, UL1 TR001414, UL1 TR001857, UL1 TR002345; National Centralized Repository for Alzheimer Disease and Related Dementias, Grant/Award Number: U24 AG21886

from cognitively-stable neurotypical participants. We found no additional benefit of using diagnose-specific atlases matching disease status. All atlases are made publicly available for the research community.

KEYWORDS

Alzheimer's disease, amyloid, dementia, Down syndrome, group atlas, joint label fusion, neurotypical

Highlight

- Down syndrome (DS) joint-label-fusion atlases provide accurate positron emission tomography (PET) amyloid measurements.
- A disorder-specific DS atlas is better than a neurotypical atlas for PET quantification.
- It is not necessary to use a disease-state-specific atlas for quantification in aged DS.
- Dorsal striatum results vary, possibly due to this region and dementia progression.

1 | INTRODUCTION

Down syndrome (DS) is a genetic disorder caused by abnormal cell division resulting in an extra copy of chromosome 21.¹ Trisomy 21 leads to developmental abnormalities impacting brain growth.² Differences include $\approx 20\%$ decrease in brain volume and an overall reduction in the cerebral and cerebellar hemispheres compared to age-matched controls.³⁻⁵ In addition, individuals with DS are at a higher risk of developing neuropathological phenotypes that are indistinguishable from Alzheimer's disease (AD), including early overproduction of amyloid.⁶ The early progression of AD in participants with DS is thought to be associated with the amyloid overexpression⁷⁻⁹ and thus measuring brain amyloid accurately may help to identify those at risk of early transition to dementia.¹⁰

Positron emission tomography (PET) has been used to identify amyloid deposition in the brain and is a widely used neuroimaging tool for AD research.^{10,11} Due to the lack of structural information in amyloid PET scans, researchers investigating regional amyloid typically obtain a magnetic resonance imaging (MRI) scan to identify regional anatomic boundaries, serving as an individual brain atlas. Often the acquisition of an MRI scan is challenging in intellectually impaired populations because of contraindications (e.g., incomplete sequences related to claustrophobia and/or general discomfort) or the data are unusable due to significant motion artifacts.¹²⁻¹⁴ When an MRI is unusable, researchers use one of several canonical brain atlases, often constructed from a single, young, healthy individual, or groups of individuals, whose brain morphometry is vastly different from those with DS.

Such atlases may not accurately reflect DS morphology thus resulting in inaccurate quantification of regional amyloid, impacting our understanding of the relationship to dementia-related disease progression.

Given the challenges researchers face in structural brain mapping and the complexity and variation in atrophy, shape, and size of the human brain, accurate structural brain templates that account for variation and represent the population accurately are required.¹⁵ Prior efforts in this area have focused on building MRI templates of tissue types for PET amyloid investigations in DS¹⁶ whereas here we build complete atlases.

In this work, we created a series of probabilistic disease-state (i.e., cognitively stable [CS-DS], mild cognitive impairment [MCI-DS], or dementia [DEM-DS]), and disorder-specific (i.e., DS) brain atlases from participants with DS. Generally, group standardized atlases are thought to reduce subject-to-subject variability compared to individual segmentations,³⁷ whereas typical individualized MRI-based FreeSurfer segmentations rely on prior information obtained through regression coefficient predictions and high-dimensional Bayesian optimizations.³⁸ For this reason, we evaluated the accuracy of using these group-based atlases to compute regional amyloid distributions by disease status compared to using individualized MRI-based segmentations or using a group atlas constructed from similar-aged cognitively stable neurotypical (CS-NT) participants. We hypothesized that using group atlases that match the disease state and disorder will result in regional amyloid measurements that are most sensitive to disease status and most consistent with the individualized MRI-based segmentations.

2 | METHODS

2.1 | Participants

Neuroimaging data of participants with DS were collected as part of the Alzheimer's Disease-Down Syndrome (ADDS), now part of the Alzheimer's Biomarkers Consortium-Down Syndrome (ABC-DS), and neurotypical (i.e., healthy) participants from the Neuroimaging Biomarkers for Cognitive Decline in Elderly with Amyloid Pathology (National Institute on Aging [NIA]) project at the University of California, Irvine (UCI). Data from 83 participants with DS (Table 1) were collected at three participating sites: Massachusetts General Hospital/Harvard University (MGH), Columbia University, and UCI. The neurotypical dataset from the NIA study consisted of 56 participants. Informed consent was obtained from all participants and their legal representatives prior to their participation.

2.1.1 | Participants' consensus diagnosis

Our sample included participants with three consensus diagnoses: CS-DS—participants who show no signs of dementia or cognitive decline; MCI-DS—participants with DS who show mild cognitive deterioration but do not satisfy the criteria for dementia; DEM-DS—participants with DS showing severe cognitive impairment. Each participant's diagnostic status was determined at a consensus case conference using a standardized assessment battery that includes a review of their health status and medical records, an assessment of their function and vocational abilities, maladaptive behaviors as well as neuropsychiatric concerns, and a direct assessment of a variety of cognitive abilities.¹⁷⁻¹⁹

2.1.2 | Image acquisition

T1-weighted MRI scans for the DS sample acquired at UCI were scanned on a Philips Achieva 3T (orientation = sagittal, TR/TE = 7.8/3.6 ms, flip angle = 7, voxel size = 1 mm³, matrix size = 256 × 256 × 176) or a Siemens Prisma 3T (orientation = sagittal, IT/TR/TE = 900/2300/3.0 ms, flip angle = 9, voxel size = 1 mm³, matrix size = 240 × 256 × 208). Both Columbia and MGH used a Siemens Prisma 3T scanner with consistent protocols. For the NIA

RESEARCH IN CONTEXT

- 1. Systematic Review:** Trisomy 21 impacts the overexpression of amyloid plaques in the brains of individuals with Down syndrome (DS) suggesting a link to the early progression of Alzheimer's disease (AD). The authors reviewed the literature in PubMed, conference publications, abstracts, and posters along with current research from the Alzheimer's Biomarkers Consortium-Down Syndrome (ABC-DS). This effort will provide a valuable tool to accurately accumulate regional positron emission tomography (PET) amyloid in DS in the absence of individual magnetic resonance imaging (MRI) scans.
- 2. Interpretation:** Our results suggest that disease and disease-specific DS atlases better match individual MRI atlases than age-matched cognitively stable neurotypical atlases, showing the need for an MRI-based DS atlas for better prediction of PET amyloid accumulations in the brains of individuals with DS.
- 3. Future Directions:** Future efforts are encouraged to focus on longitudinal group data to improve our understanding of the impact of DS-related brain atrophy and structural changes on the accuracy of DS atlases' amyloid measurements.

study, participants were scanned at UCI on a Siemens Prisma 3T (orientation = coronal, IT/TR/TE = 902/2300/2.38 ms, flip angle = 8, voxel size = 0.8 mm³, matrix size = 320 × 320 × 240).

¹⁸F-AV-45 (florbetapir) PET scans of the UCI DS sample were acquired on a high resolution research tomograph (HRRT; voxels = 1.2 mm³, matrix = 256 × 256 × 207, reconstruction = OP-OSEM3D) at Columbia on a Siemens Biograph64 mCT (voxels = 1.0 × 1.0 × 2.0 mm, matrix = 400 × 400 × 436, reconstruction = OSEM3D+TOF 4i21s), and MGH on a Siemens Biograph mMR (voxels = 2.1 × 2.1 × 2.0 mm, matrix = 344 × 344 × 127, reconstruction = OP-OSEM 3i21s). Image acquisition followed the Alzheimer's Disease Neuroimaging Initiative^{16,20,21} protocol. PET reconstructions were performed with all corrections as implemented on each platform.

TABLE 1 Participant characteristics showing the total sample size (N), sex, age mean ± standard deviation, and minimum/maximum age in years

Diagnosis	N	Sex	Mean age ± SD (years)	[min,max] Age (years)
Down syndrome (DS)	83	29F/54M	50 ± 6.8	[40,67]
Cognitively stable (CS-DS)	53	21F/32M	48 ± 5.9	[40,62]
Mild cognitive impairment (MCI-DS)	19	2F/17M	54 ± 6.5	[44,67]
Dementia (DEM-DS)	11	6F/5M	55 ± 6.6	[44,65]
Cognitively stable neurotypicals (CS-NT)	56	43F/13M	72 ± 5.1	[61,81]

PET scan processing followed the methods described in Keator et al.,²² consisting of spatial resolution matching across the three imaging platforms, realignment and averaging of the PET frames, co-registration with the structural MRI, and standardized uptake value ratio (SUVR) scaling using each participant's cerebellar gray reference region.

2.2 | Atlas creation

In this study, we created a series of brain atlases using the Advanced Normalization Tools' (ANTs version 2.2.0; RRID:SCR_004757) joint label fusion algorithm.^{23,24} The joint label fusion atlases were created by propagating the individual MRI-based segmentations computed with FreeSurfer (FS6 version 6.0; RRID:SCR_001847) and the Desikan/Killiany atlas.^{25–28} Segmentations were visually checked for accuracy and corrected when necessary using procedures from FreeSurfer.²⁹ The volumetric aparc+aseg segmentations from FreeSurfer and associated T1-weighted MRIs were used in creating the joint label fusion atlases. To align the PET scan images with the joint label fusion atlases, ANTs' symmetric diffeomorphic image registration algorithm was used to register each participant's structural MRI to each joint label fusion atlas and apply the resulting deformations to the coregistered PET scan. PET scan region-of-interest (ROI) average SUVR values were then extracted from each joint label fusion atlas and from the individual MRI-based FreeSurfer segmentations for the comparisons presented in Section 3 (Figure 1). The following regions were chosen based on existing AD literature implicating them in the progression of the disease: inferior parietal, lateral occipital, superior/rostral-medial frontal, medial/inferior/superior temporal, anterior/posterior cingulate, dorsal striatum, medial/lateral orbitofrontal, hippocampus, and entorhinal cortex.

2.2.1 | Disorder and disease-state-specific group (DSG) atlas

To evaluate the accuracy of using a joint label fusion group atlas within disorder (i.e., DS) and consistent with a participant's disease status (e.g., CS-DS, MCI-DS, DEM-DS), disease-state-specific (DSG) atlases were constructed using individual MRI-based segmentations separately for each consensus diagnosis: CS-DS, MCI-DS, and DEM-DS (see Table 1). For the PET comparisons, we created a series of DSG atlases, leaving one participant out in a cross-validation paradigm, to compare to their individual MRI-based PET ROI averages. This was done to prevent bias in the joint label fusion-derived regional PET measures as would be the case if the participant's data being evaluated were used in constructing the joint label fusion atlas.

2.2.2 | Disorder-specific cognitively stable Down syndrome (CS-DS) group atlas

In Section 2.2.1 we constructed group atlases that took into account the disease status in DS. Here we evaluated whether atlases

constructed from MCI-DS and DEM-DS (seen in Section 2.2.1) are beneficial or whether an atlas created from cognitively stable individuals with DS (CS-DS) would still have similar results compared to individual MRI-based segmentation. To evaluate the CS-DS atlas, we compared individual MRI-based PET ROI averages in participants who had either a consensus-based diagnosis of MCI-DS or DEM-DS and not CS-DS; because this comparison was performed in Section 2.2.1, we did not need to use leaving-one-out in a cross-validation paradigm.

2.2.3 | Cognitively stable neurotypical (CS-NT) group atlas

In Sections 2.2.1 and 2.2.2 we evaluated group atlases that take into account the disease status and disorder. Here we construct a group atlas from the cognitively stable neurotypical (CS-NT) participants to evaluate whether accounting for the disorder (e.g., DS) or disease status is necessary for accurate PET ROI averages compared to the individual MRI method. Similar to the CS-DS atlas, we built an atlas reflecting the aged brain (72 ± 5.1 years) of cognitively stable participants without DS. For evaluations of the CS-NT atlas, we compare the individual MRI-based PET ROI averages in each of the diagnostic groups (i.e., CS-DS, MCI-DS, and DEM-DS).

2.3 | PET ROI analysis

To quantify differences in the regional average SUVR values between the three diagnostic groups, we built fixed-effects linear regression models for each ROI separately using RStudio (version 1.1447; RRID:SCR_001905). The dependent variable was the difference in amyloid load between our atlases (i.e., DSG, CS-DS, CS-NT) and individualized MRI-based segmentations as a function of average amyloid load between the two atlases, diagnosis, and the interaction between the average amyloid load and diagnosis. Results (Section 3) are illustrated using Bland Altman plots.^{30,31}

3 | RESULTS

3.1 | Atlas structure comparisons

To quantify the overall structural differences between atlases, we computed the mean squared error (MSE) of the disorder and disease-state-specific group (DSG), CS-DS, and CS-NT atlases compared to individualized MRI-based segmentations. MSE scores were normalized to the MSE score of comparing the joint label fusion atlas to a matrix of zeros and scaled to percentage. High MSE scores indicate a poor match between the anatomical labels in joint label fusion atlases and individualized MRI-based segmentations. MSE scores were compared across the atlases (Section 3.1.1) using one-way analysis of variance (ANOVA) and Tukey's honest significant difference (TukeyHSD) tests in RStudio (version 1.1447; RRID:SCR_001905). *P*-values from the

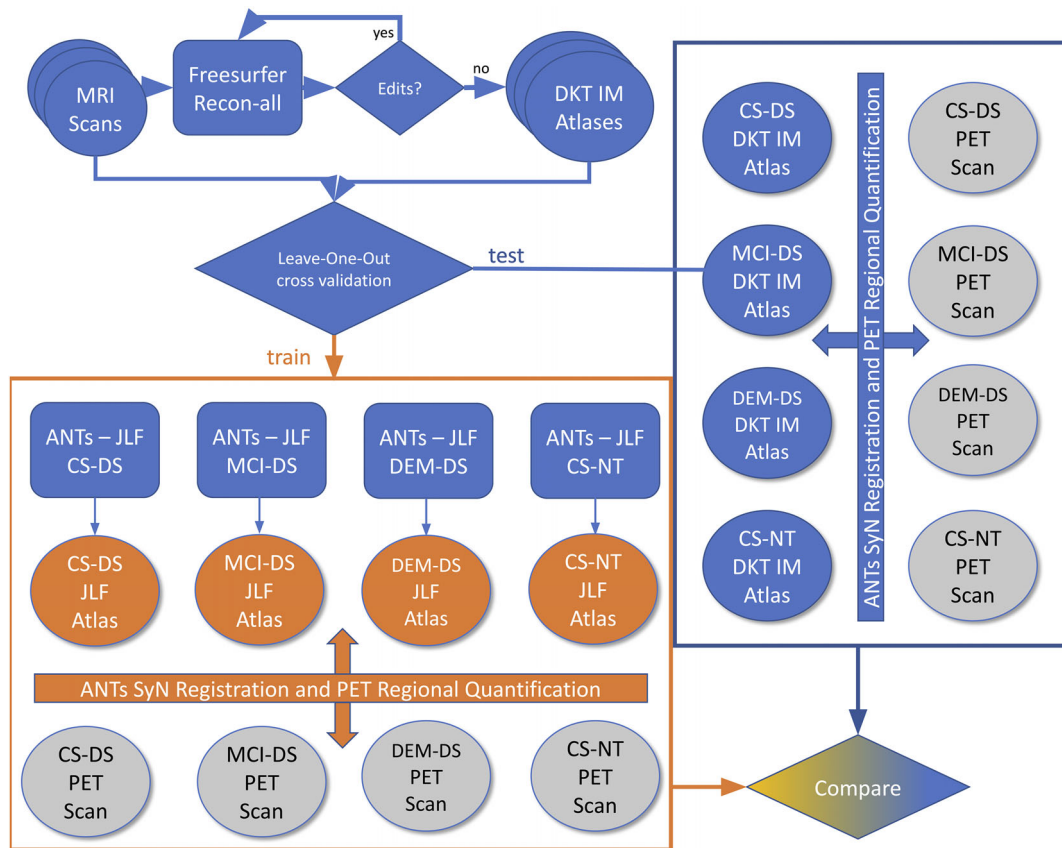


FIGURE 1 A flow diagram visualizing the probabilistic atlases' creation and the alignment of the atlases with the amyloid positron emission tomography (PET) scans. In addition, the diagram shows the comparisons of each of the atlases with the Desikan/Killiany (DKT) individual magnetic resonance imaging (MRI) segmentation (IM) atlas in a leave-one-out cross-validation (LOOCV) paradigm. ANTs, Advanced Normalization Tools; CS-DS, cognitively stable Down syndrome; CS-NT, cognitively stable neurotypical; DEM-DS, dementia Down syndrome; JLF, joint label fusion; MCI-DS, mild cognitive impairment Down syndrome

overall ANOVA were adjusted using the Bonferroni-Hommel method.³² A visual example of the DSG, CS-DS, and CS-NT atlases compared to a selected individualized MRI-based atlas is included in the supporting information (S1).

3.1.1 | Comparisons across atlases within diagnostic groups

Here we evaluate the overall difference in ROI segmentations between individualized FreeSurfer MRI-based segmentations and each group joint label fusion atlas across diagnostic groups. The overall ANOVA models of CS-DS (Figure 2A) and MCI-DS (Figure 2B) groups were not significantly different across atlases. In comparison, the DEM-DS overall model was significantly different across the atlases ($F(2,30) = 8.669$, $P_{adj.} < .003$; Figure 2C). A post hoc Tukey test showed that, in the DEM-DS group, both the CS-DS and the CS-NT atlases had an MSE score that was significantly different from the DSG atlas (CS-DS vs. DSG [$t(20) = -8.013$, $P_{adj.} < .006$]; CS-NT vs. DSG [$t(20) = -9.001$, $P_{adj.} < .002$]), while no significant differences were observed between the CS-DS and CS-NT atlases.

In summary, both the CS-DS and MCI-DS groups' average MSE scores remained consistent across each atlas, indicating no significant structural differences between the group atlases and individualized MRI-based segmentations. Interestingly, in the DEM-DS group, the DSG atlas had a significantly higher mean MSE score than both CS-DS and CS-NT atlases compared to individualized MRI-based segmentations, suggesting more structural differences between the DSG atlas and the FreeSurfer segmentations than in either CS-DS or CS-NT atlases. Upon further interrogation, we find the structural differences are predominantly on the region borders (supporting information S1) and that differences in the DEM-DS group (Figure 2C) are likely due to brain atrophy resulting in the DSG atlas being less consistent with each individualized MRI-based segmentation.

3.2 | PET ROI comparisons

3.2.1 | DSG versus individual MRI-based atlases

To investigate whether the structural differences found in Section 3.1 affect our PET regional averages, we evaluate differences in regional

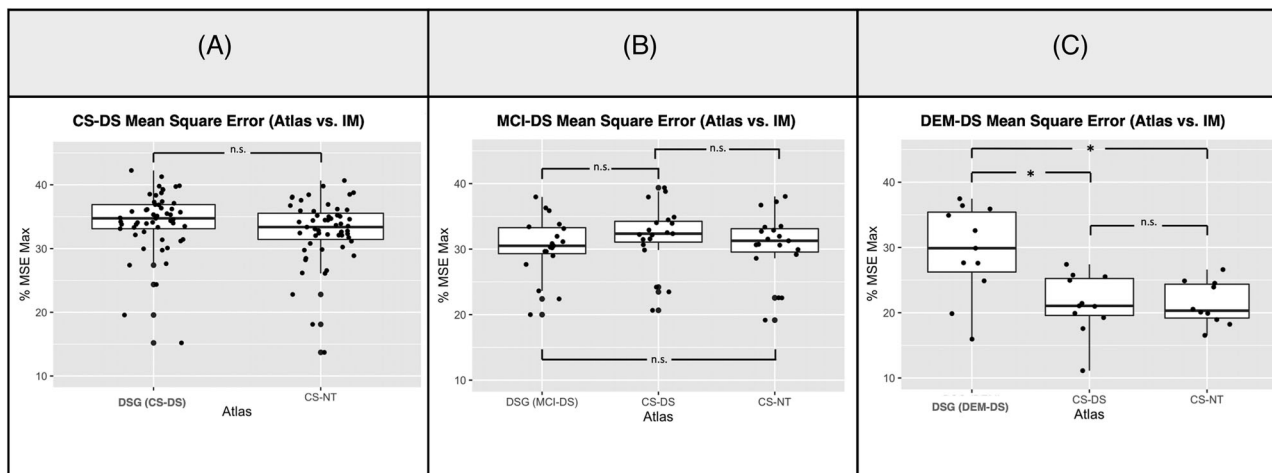


FIGURE 2 Mean squared error (MSE) by atlas. A higher percentage of MSE score indicates a worse match between our atlas and the individual magnetic resonance imaging (MRI)-based FreeSurfer segmentations (IM). Asterisks identify results that are significant at $P < .05$ after adjusting for the P -value, whereas “n.s.” indicates non-significant. CS-DS, cognitively stable Down syndrome; CS-NT, cognitively stable neurotypical; DEM-DS, dementia Down syndrome; MCI-DS, mild cognitive impairment

PET measurements between the DSG and individual MRI-based atlases using fixed-effects linear regression. Participants' data within ± 3 standard deviations were included in the analysis and reported. Results are visualized using Bland Altman plots (Figure 3A).³³ Regression lines for each diagnosis are shown as a function of the difference (DSG-individual MRI-based atlases) between PET ROI averages computed using each atlas (y-axis) and the average amyloid load across both atlases (x-axis). Differences closer to zero indicate better correspondence between average regional amyloid from both atlases. Regression lines with positive slope indicate increasing differences between the two atlases as a function of higher amyloid whereas lines with zero slope and zero difference indicate perfect correspondence across the range of amyloid between both atlases. Prior to P -value adjustments, the dorsal striatum, lateral orbitofrontal cortex, and anterior cingulate were significantly different in PET ROI mean values between atlases. After adjusting for multiple comparisons the dorsal striatum remained significant.

3.2.2 | PET ROI comparisons CS-DS versus individual MRI-based atlases

The results from Section 3.2.1 suggest that PET amyloid measures are reasonably consistent between DSG and individual MRI-based atlases with the exception of a few regions. Here we evaluate whether we need to account for disease status by comparing the atlas of cognitively stable participants with DS (CS-DS) and computing PET averages in participants with the diagnoses of MCI-DS or DEM-DS. We expect that due to disease-related atrophy and comorbidities, using a group atlas based on those who are cognitively stable would result in less consistent matches with individual MRI-based segmentations compared to the DSG atlas. The analysis was performed using the same approach as the comparisons in Section 3.2.1. Significant regions included the dorsal

striatum, inferior temporal, middle temporal, and lateral orbitofrontal cortex (Figure 3B). Similar to the DSG atlas results, the dorsal striatum was the only region to survive the P -value adjustment although, in this analysis, we see temporal regions, known to be among the most affected by disease-related atrophy in AD, significant before adjustment. The Bland Altman plots (Figure 3B) are reasonably consistent between MCI-DS and DEM-DS groups suggesting it may not be necessary to use atlases that account for disease severity.

3.2.3 | PET ROI comparisons CS-NT versus individual MRI-based atlases

Expanding upon the results from Sections 3.2.1 and 3.2.2, we report on similar experiments using an atlas made from cognitively stable neurotypical participants (CS-NT) of similar age. Due to brain morphological differences in DS, we expect the results when using the CS-NT atlas to be less consistent with the individual MRI-based atlases. Interestingly, similar regions to both the DSG and CS-DS atlas comparisons were identified as different from the individual MRI-based atlas at the $P < .05$ unadjusted threshold: dorsal striatum, middle temporal, inferior temporal along with one additional region: entorhinal cortex (Figure 3C). Further, two additional regions approached significance: superior temporal and hippocampus. After P -value adjustments, both the dorsal striatum and middle temporal lobe remained significant, with the entorhinal cortex approaching an adjusted significance level of $P < .05$.

3.3 | Amyloid by diagnostic group comparisons

In Sections 3.1–3.2, we evaluated differences in atlas structure and regional amyloid average values, across our group atlases and the indi-

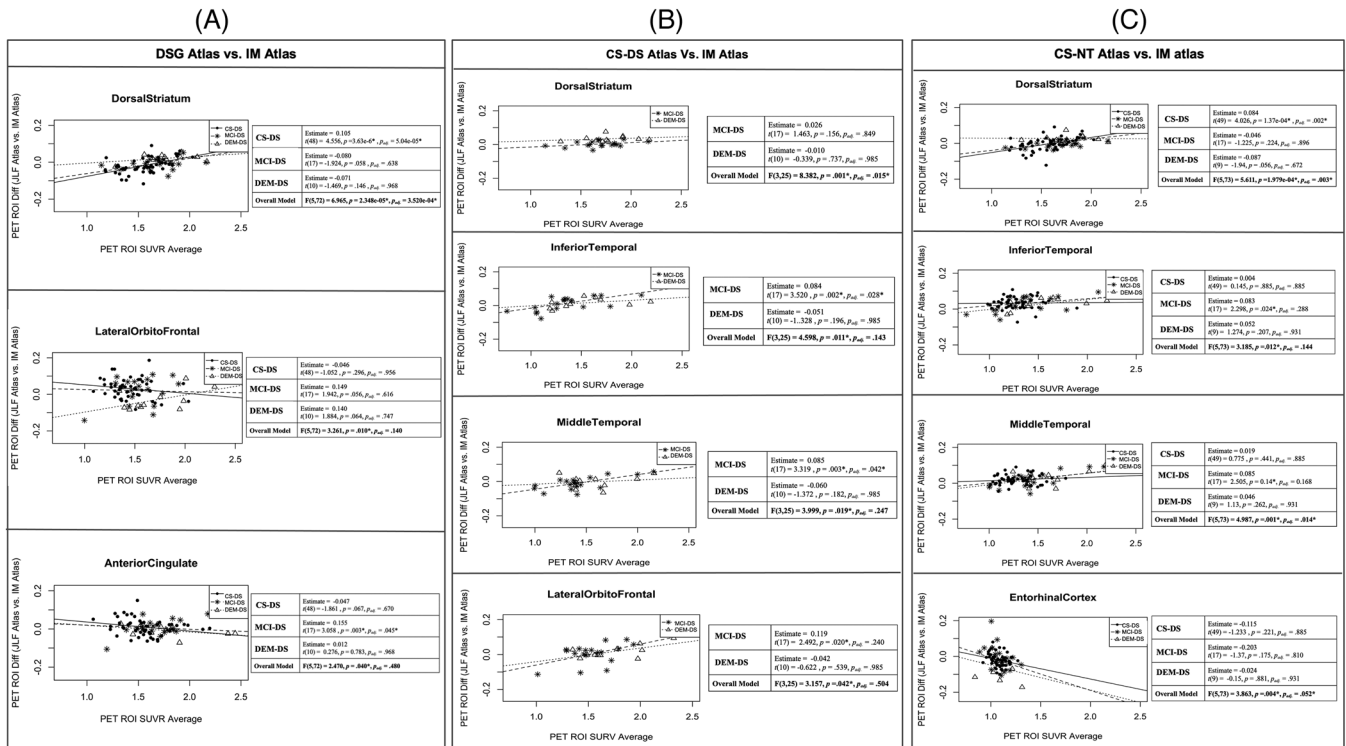


FIGURE 3 Bland Altman plots of significant regional differences in average amyloid and the corresponding linear regression model statistics are shown for each region of interest (ROI). Each plot illustrates the relationship between the difference in amyloid measurements on the y-axis and the average amyloid load on the x-axis. Regression lines with a positive slope indicate an increasing difference between the two atlases as a function of higher amyloid. Only results from the regression model statistics of ROI that were significant at the $P < .05$ unadjusted threshold are reported here. A, Results of significant regional differences in average amyloid between diagnosis-specific group (DSG) and individual magnetic resonance imaging (IM) atlases. B, Results of significant regional differences in average amyloid between cognitively stable Down syndrome (CS-DS) and IM atlases. C, Results of significant regional differences in average amyloid between cognitively stable neurotypical (CS-NT) and IM atlases. DEM-DS, dementia Down syndrome; MCI-DS, mild cognitive impairment; PET, positron emission tomography

vidual MRI-based segmentations. We found some differences in structure and amyloid average values but it is unclear whether these differences would result in alternative inferences about disease progression when using a group atlas instead of individualized MRI-based FreeSurfer segmentations. In this section, we look at this question explicitly by focusing on pairwise comparisons typically used to evaluate regional amyloid as a function of disease state (e.g., DEM-DS vs. MCI-DS, MCI-DS vs. CS-DS, DEM-DS vs. CS-DS). To perform these comparisons, we use fixed-effects linear regression and include age, gender, and disease status as regressors against each region's amyloid average, for each of the atlases (e.g., DSG, CS-DS, CS-NT, and individual MRI-based atlases). The results are shown in Table 2 and include regions for which the inferences would have changed at the $P < .05$ unadjusted significance level, either false positives or negatives, compared to individual MRI-based atlases. Comparing DEM-DS to the CS-DS group, we find that no inferences would have changed using any of the group atlases compared to the individual MRI-based atlases. However, comparing the MCI-DS and DEM-DS groups, we see that our inference about lateral and medial orbitofrontal would change. For lateral orbitofrontal, if we used a group atlas made from cognitively stable participants with DS (CS-DS) or neurotypicals (i.e., without DS; CS-NT), we would infer amyloid load is significantly different between those

with a diagnosis of MCI-DS versus DEM-DS whereas if we used the DSG atlas our inference would be the same as with individual MRI-based atlases. For medial orbitofrontal, we see a change when using any of the alternative group atlases, going from non-significant with individual MRI-based to significant with the group atlases. Comparing the MCI-DS and CS-DS groups we see many inferences that would have changed. Specifically, amyloid load in lateral occipital, rostral middle frontal, prefrontal cortex, medial orbitofrontal cortex, dorsal striatum, and anterior cingulate were all significantly different between the two groups using the individual MRI-based atlases yet mostly (exception: rostral middle frontal using CS-DS atlas) became non-significant when using any of the group atlases. Further, the hippocampus was non-significant with the individual MRI-based atlas but became significant using the group atlases.

4 | DISCUSSION

In this study, we created a series of probabilistic group atlases (i.e., DSG, CS-DS, and CS-NT) and evaluated their accuracy compared to individualized MRI-based FreeSurfer segmentations when measuring regional amyloid. We hypothesized that using DSG atlases would best match

TABLE 2 Group amyloid comparisons by region and atlas

Comparison	Region	IM			DSG atlases			CS-DS atlases			CS-NT atlases		
		t(78)	SE	P	t(78)	SE	P	t(78)	SE	P	t(78)	SE	P
DEM-DS vs. MCI-DS	Lateral orbito frontal	1.545	0.085	.063	1.440	0.091	.077	2.137	0.091	.018*	2.065	0.091	.021*
	Medial orbito frontal	1.134	0.095	.130	1.685	0.099	.048*	1.801	0.098	.038*	1.782	0.097	.039*
MCI-DS vs. CS-DS	Lateral occipital	2.119	0.062	.019*	1.153	0.072	.126	1.154	0.073	.126	0.990	0.071	.163
	Rostral middle frontal	2.024	0.081	.023*	1.552	0.084	.062	1.794	0.085	.038*	1.475	0.088	.072
	Prefrontal	1.995	0.070	.025*	1.405	0.071	.082	1.522	0.072	.066	1.340	0.073	.092
	Medial orbito frontal	1.860	0.070	.033*	1.447	0.072	.076	1.108	0.072	.136	1.407	0.071	.082
	Dorsal striatum	1.832	0.062	.035*	1.512	0.069	.067	1.652	0.069	.051	1.394	0.068	.084
	Anterior cingulate	1.731	0.071	.044*	1.168	0.079	.123	0.966	0.079	.168	1.137	0.080	.129
	Hippocampus	1.331	0.035	.093	1.892	0.036	.031*	2.237	0.036	.014*	2.188	0.037	.016*
DEM-DS vs. CS-DS	No changed inferences												

Note: Regions are included if inferences changed from individual MRI segmentation (IM) when using a group atlas. Regions with significant differences surviving the $P < .05$ unadjusted threshold are indicated by *. Reported in the table are the group contrast, brain region (i.e., ROI), t-statistic (t), standard error (SE), P-value (P), and adjusted P-value (p_{adj}), respectively.

Abbreviations: CS-DS, cognitively stable Down syndrome; CS-NT, cognitively stable neurotypical; DEM-DS, dementia Down syndrome; DSG, diagnosis-specific group; MCI-DS, mild cognitive impairment; MRI, magnetic resonance imaging; ROI, region of interest

the individualized MRI-based segmentation measurements, followed by CS-DS, because they account for disorder-specific differences in brain morphology. In evaluating the structural differences in the group atlases compared to the individualized MRI-based segmentations, we found higher MSE values in the DEM-DS group when using the DSG atlas driven primarily by differences in each anatomical region's boundaries. With respect to regional amyloid measurements, we found, generally, that both DSG and CS-DS atlases did quite well in matching individualized MRI-based atlas measurements with the exception of a few regions identified (e.g., dorsal striatum across all atlases). As expected, we found increasingly more differences from the individualized MRI-based atlases as we moved from using disease-state atlases (DSG) to a disorder-specific atlas (CS-DS) and finally the neurotypical atlas (CS-NT).

Investigating AD progression using amyloid PET relies on accurately quantifying regional amyloid differences across cohorts. We, therefore, evaluated differences between diagnostic groups when using each of the atlases, focusing on instances when our interpretation would have changed, and found quite a few instances where one might implicate different regions in AD progression if using the group atlases (Section 3.3). These effects were confined to diagnoses that were adjacent to one another in terms of disease progression (e.g., MCI-DS vs. CS-DS, DEM-DS vs. MCI-DS) which likely have more overlap in their amyloid distributions and smaller differences across groups.

More specifically, the dorsal striatum resulted in an alternative inference in the transition from CS-DS to MCI-DS when using the group atlases in addition to being the only region to survive the adjusted P-value thresholds (Section 3.2). Prior studies suggest that early amyloid binding in dorsal striatum foreshadows the onset of dementia^{22,31,34,35} and that brain atrophy in striatal regions in individuals with DS are consistent with findings from AD studies in neurotypical populations.³⁶ In

vivo human neuroimaging studies in DS have also shown presence of amyloid in the striatum around 40 years of age.^{37,38} Because regional amyloid retention positively correlates with regional cell loss and brain atrophy,³⁹ we expect the early amyloid load and structural atrophy in the dorsal striatum to be associated with increased variability across our participants in this region.

Our study had several limitations. First, it is unclear whether individualized MRI-based FreeSurfer segmentations are capturing regional boundaries more accurately than the group atlases. We suspect FreeSurfer is better able to capture individual variability in boundaries because they are based on segmenting an individual's MRI; however, there may be additional variability introduced through the complex optimizations performed by FreeSurfer in detecting these boundaries. Another limitation is the neurotypical sample age which is, on average, older than our DS sample. Elderly neurotypical participants might reflect greater age-associated brain atrophy compared to age-matched neurotypical participants.⁴² Further, our relatively small DEM-DS sample may have hindered our ability to accurately capture population-level brain structural variability in this group. Future efforts are encouraged to compare DEM-DS atlas, with a larger sample size, to an atlas constructed from age-matched neurotypical individuals with AD dementia.

In summary, both the disease-specific and diagnosis-specific atlases (i.e., DSG and CS-DS) performed better in replicating the regional amyloid measurements of the individualized MRI-based FreeSurfer segmentations than the neurotypical atlas (CS-NT). Overall, we suggest using the CS-DS atlas because it appears to be as accurate as the DSG atlas for use in this population and better captures the overall variability in atrophy across the diagnostic groups. Each of the atlases (DSG, CS-DS, and CS-NT), the posterior probability maps for each ROI from the joint-label-fusion algorithm, and the scripts to create

the atlases along with a Neurodocker (RRID:SCR_017426) image containing the required software are made publicly available at http://www.nitrc.org/projects/ds_brainatlas/. The DS dataset used for this study is available from the ABC-DS consortium through the Laboratory of Neuro Imaging Image and Data Archive database.⁴³ Future work will focus on longitudinal group atlases to better understand the effects of disease-related brain changes on the accuracy of group atlas-based measurements and on building group atlases of younger cohorts with DS.

ACKNOWLEDGMENTS

The preparation of this manuscript was made possible from data obtained by the Alzheimer's Disease in Down Syndrome (ADDS) component of the Alzheimer's Biomarkers Consortium-Down Syndrome (ABC-DS), a longitudinal study of Alzheimer disease biomarkers in adults with Down syndrome is supported by grants from the National Institute on Aging (NIA; U01AG051412-01 Schupf, Lott, Silverman) and Eunice Kennedy Shriver National Institute of Child Health and Human Development (NICHD). The Co-Principal Investigators of the ADDS component of the ABC-DS program are Nicole Schupf, PhD, Dr. PH. (Columbia University), Ira Lott, MD, and Wayne Silverman, PhD (UC Irvine). Co-Principal Investigators of the NiAD ABC-DS component are Benjamin Handen, PhD and William Klunk, MD, PhD (University of Pittsburgh), and Bradley Christian, PhD (University of Wisconsin-Madison). Neurotypical data were collected under the Neuroimaging biomarkers for cognitive decline in elderly with amyloid pathology (NIA) grant from the National Institute on Aging (R01AG053555 Yassa, Gillen). The atlases and data processing scripts were made available using the recommendations for FAIR data, tools, and techniques from ReproNim: A Center for Reproducible Neuroimaging Computation supported by a grant from the National Institute of Biomedical Imaging and Bioengineering (P41 EB019936; Kennedy). The Alzheimer's Biomarkers Consortium-Down Syndrome (ABC-DS) is funded by the National Institute on Aging and the National Institute for Child Health and Human Development (U01 AG051406 and U01 AG051412). The work contained in this publication was also supported through the following National Institutes of Health Programs: The Alzheimer's Disease Research Centers Program (P50 AG008702, P30 AG062421, P50 AG16537, P50 AG005133, P50 AG005681, and P30 AG062715), the Eunice Kennedy Shriver Intellectual and Developmental Disabilities Research Centers Program (U54 HD090256 and U54 HD087011), the National Centers for Advancing Translational Sciences (UL1 TR001873, UL1 TR002373, UL1 TR001414, UL1 TR001857, UL1 TR002345), the National Centralized Repository for Alzheimer Disease and Related Dementias (U24 AG21886), and DS-Connect® (The Down Syndrome Registry) supported by the Eunice Kennedy Shriver National Institute of Child Health and Human Development. The authors thank the ABC-DS study participants (adults with Down syndrome and their siblings), their families and care providers, and the ABC-DS research and support staff for their invaluable contributions to this study. The content is the sole responsibility of the authors and does not necessarily represent the official views of the NIH.

CONFLICTS OF INTEREST

The authors do not have any conflict of interest to declare.

ALZHEIMER'S BIOMARKER CONSORTIUM- DOWN SYNDROME (ABC-DS) INVESTIGATORS

Howard J. Aizenstein, MD PhD; Beau M. Ances, MD PhD; Howard F. Andrews, PhD; Karen Bell, MD; Rasmus M. Birn, PhD; Adam M. Brickman, PhD; Peter Bulova, MD; Amrita Cheema, PhD; Kewei Chen, PhD; Bradley T. Christian, PhD; Isabel Clare, PhD; Lorraine Clark, PhD; Ann D. Cohen, PhD; John N. Constantino, MD; Eric W. Doran, MS; Anne Fagan, PhD; Eleanor Feingold, PhD; Tatiana M. Foroud, PhD; Benjamin L. Handen, PhD; Sigal L. Hartley, PhD; Elizabeth Head, PhD; Rachel Henson, PhD; Christy Hom, PhD; Lawrence Honig, MD; Milos D. Ikonovic, MD; Sterling C. Johnson, PhD; Courtney Jordan, RN; M. Ilyas Kamboh, PhD; David Keator, PhD; William E. Klunk, MD PhD; Julia K. Kofler, MD; William Charles Kreisler, MD; Sharon J. Krinsky-McHale, PhD; Florence Lai, MD; Patrick Lao, PhD; Charles Laymon, PhD; Joseph Hyungwoo Lee, PhD; Ira T. Lott, MD; Victoria Lupson, PhD; Mark Mapstone, PhD; Chester A. Mathis, PhD; Davneet Singh Minhas, PhD; Neellesh Nadkarni, MD; Sid O'Bryant, PhD; Deborah Pang, MPH; Melissa Petersen, PhD; Julie C. Price, PhD; Margaret Pulsifer, PhD; Eric Reiman, MD; Batool Rizvi, MS; Herminia Diana Rosas, MD; Nicole Schupf, PhD; Wayne P. Silverman, PhD; Dana L. Tudorascu, PhD; Rameshwari Tumuluru, MD; Benjamin Tycko, MD PhD; Badri Varadarajan, PhD; Desiree A. White, PhD; Michael A. Yassa, PhD; Shahid Zaman, MD PhD; Fan Zhang, PhD.

ORCID

Nazek Queder  <https://orcid.org/0000-0001-6268-862X>

Michael A. Yassa  <https://orcid.org/0000-0002-8635-1498>

David B. Keator  <https://orcid.org/0000-0001-5281-5576>

REFERENCES

1. Parker SE, Mai CT, Canfield MA, et al. Updated National Birth Prevalence estimates for selected birth defects in the United States, 2004–2006. *Birth Defects Res A Clin Mol Teratol.* 2010;88(12):1008–1016.
2. Lee NR, Adeyemi EI, Lin A, et al. Dissociations in cortical morphometry in youth with down syndrome: evidence for reduced surface area but increased thickness. *Cereb Cortex.* 2016;26(7):2982–2990.
3. Raz N, Torres IJ, Briggs SD, et al. Selective neuroanatomic abnormalities in Down's syndrome and their cognitive correlates: evidence from MRI morphometry. *Neurology.* 1995;45(2):356–366.
4. Rodrigues M, Nunes J, Figueiredo S, Martins de Campos A, Geraldo AF. Neuroimaging assessment in Down syndrome: a pictorial review. *Insights Imaging.* 2019;10(1):52.
5. Weis S, Weber G, Neuhold A, Rett A. Down syndrome: MR quantification of brain structures and comparison with normal control subjects. *AJNR Am J Neuroradiol.* 1991;12(6):1207–1211.
6. Strydom A, Coppus A, Blesa R, et al. Alzheimer's disease in Down syndrome: An overlooked population for prevention trials. *Alzheimers Dement.* 2018;4:703–713.
7. Annus T, Wilson LR, Hong YT, et al. The pattern of amyloid accumulation in the brains of adults with Down syndrome. *Alzheimers Dement.* 2016;12(5):538–545.
8. Cole JH, Annus T, Wilson LR, et al. Brain-predicted age in Down syndrome is associated with beta amyloid deposition and cognitive decline. *Neurobiol Aging.* 2017;56:41–49.

9. Mann DM, Jones D, Prinja D, Purkiss MS. The prevalence of amyloid (A4) protein deposits within the cerebral and cerebellar cortex in Down's syndrome and Alzheimer's disease. *Acta Neuropathol.* 1990;80(3):318-327.
10. Keator DB, Doran E, Taylor L, et al. Brain amyloid and the transition to dementia in Down syndrome. *Alzheimers Dement.* 2020;12(1):e12126.
11. Rabinovici GD, Jagust WJ. Amyloid imaging in aging and dementia: testing the amyloid hypothesis in vivo. *Behav Neurol.* 2009;21(1):117-128.
12. Ali A, Scior K, Ratti V, Strydom A, King M, Hassiotis A. Discrimination and other barriers to accessing health care: perspectives of patients with mild and moderate intellectual disability and their carers. *PLoS One.* 2013;8(8):e70855.
13. Brockmeyer D. Down syndrome and craniovertebral instability. Topic review and treatment recommendations. *Pediatr Neurosurg.* 1999;31(2):71-77.
14. Wullink M, Veldhuijzen W, Lantman-de Valk HM van S, Metsemakers JFM, Dinant GJ. Doctor-patient communication with people with intellectual disability—a qualitative study. *BMC Fam Pract.* 2009;10:82.
15. New approaches in brain morphometry. *Am J Geriatr Psychiatry.* 2002;10(1):13-23.
16. Lao PJ, Handen BL, Betthausen TJ, et al. Imaging neurodegeneration in Down syndrome: brain templates for amyloid burden and tissue segmentation. *Brain Imaging Behav.* 2019;13(2):345-353.
17. Silverman W, Schupf N, Zigman W, et al. Dementia in adults with mental retardation: assessment at a single point in time. *Am J Ment Retard.* 2004;109(2):111. [https://doi.org/10.1352/0895-8017\(2004\)109<111:diawmr>2.0.co;2](https://doi.org/10.1352/0895-8017(2004)109<111:diawmr>2.0.co;2)
18. Silverman WP, Zigman WB, Krinsky-McHale SJ, Ryan R, Schupf N. Intellectual disability, mild cognitive impairment, and risk for dementia. *J Policy Pract Intellec Disabil.* 2013;10(3):245-251. <https://doi.org/10.1111/jppi.12042>
19. Krinsky-McHale SJ, Silverman W. Dementia and mild cognitive impairment in adults with intellectual disability: issues of diagnosis. *Dev Disabil Res Rev.* 2013;18(1):31-42.
20. ADNI. Accessed November 29, 2021. <http://www.adni-info.org/>
21. Landau SM, Breault C, Joshi AD, et al. Amyloid- β imaging with Pittsburgh compound B and florbetapir: comparing radiotracers and quantification methods. *J Nucl Med.* 2013;54(1):70-77.
22. Keator DB, Phelan MJ, Taylor L, et al. Down syndrome: distribution of brain amyloid in mild cognitive impairment. *Alzheimers Dement.* 2020;12(1):e12013.
23. Avants BB, Tustison NJ, Song G, Cook PA, Klein A, Gee JC. A reproducible evaluation of ANTs similarity metric performance in brain image registration. *Neuroimage.* 2011;54(3):2033-2044.
24. Wang H, Yushkevich PA. Multi-atlas segmentation with joint label fusion and corrective learning—an open source implementation. *Front Neuroinform.* 2013;7:27.
25. Desikan RS, Ségonne F, Fischl B, et al. An automated labeling system for subdividing the human cerebral cortex on MRI scans into gyral based regions of interest. *Neuroimage.* 2006;31(3):968-980.
26. Fischl B, Salat DH, Busa E, et al. Whole brain segmentation: automated labeling of neuroanatomical structures in the human brain. *Neuron.* 2002;33(3):341-355.
27. Fischl B, van der Kouwe A, Destrieux C, et al. Automatically parcellating the human cerebral cortex. *Cereb Cortex.* 2004;14(1):11-22.
28. FreeSurfer. Accessed November 29, 2021. <https://surfer.nmr.mgh.harvard.edu/>
29. FsTutorial/TroubleshootingData – Free Surfer Wiki. Accessed December 14, 2020. <https://surfer.nmr.mgh.harvard.edu/fswiki/FsTutorial/TroubleshootingData>
30. Bland JM, Martin Bland J, Altman D. Statistical methods for assessing agreement between two methods of clinical measurement. *The Lancet.* 1986;327(8476):307-310. [https://doi.org/10.1016/s0140-6736\(86\)90837-8](https://doi.org/10.1016/s0140-6736(86)90837-8)
31. Cardemil F. Comparison analysis and applications of the Bland-Altman method: correlation or agreement? *Medwave.* 2017;17(01):e6852-e6852. <https://doi.org/10.5867/medwave.2016.01.6852>
32. Hommel G. A stagewise rejective multiple test procedure based on a modified Bonferroni test. *Biometrika.* 1988;75(2):383-386. <https://doi.org/10.1093/biomet/75.2.383>
33. Giavarina D. Understanding Bland Altman analysis. *Biochemia Medica.* 2015;25(2):141-151. doi:10.11613/bm.2015.015
34. Abrahamson EE, Head E, Lott IT, et al. Neuropathological correlates of amyloid PET imaging in Down syndrome. *Dev Neurobiol.* 2019;79(7):750-766.
35. Klunk WE, Price JC, Mathis CA, et al. Amyloid deposition begins in the striatum of presenilin-1 mutation carriers from two unrelated pedigrees. *J Neurosci.* 2007;27(23):6174-6184.
36. Annus T, Wilson LR, Acosta-Cabronero J, et al. The Down syndrome brain in the presence and absence of fibrillar β -amyloidosis. *Neurobiol Aging.* 2017;53:11-19.
37. Handen BL, Cohen AD, Channamalappa U, et al. Imaging brain amyloid in nondemented young adults with Down syndrome using Pittsburgh compound B. *Alzheimers Dement.* 2012;8(6):496-501.
38. Hartley SL, Handen BL, Devenny DA, et al. Cognitive functioning in relation to brain amyloid- β in healthy adults with Down syndrome. *Brain.* 2014;137(Pt 9):2556-2563.
39. Teipel SJ, Hampel H. Neuroanatomy of Down syndrome in vivo: a model of preclinical Alzheimer's disease. *Behavior Genetics.* 2006;36(3):405-415. <https://doi.org/10.1007/s10519-006-9047-x>
40. Thompson P, Mega MS, Toga AW. Disease-specific probabilistic brain atlases. *Proc IEEE Comput Soc Conf Comput Vis Pattern Recognit.* 2000;2000:227-234.
41. Chen G, Xiao Y, Taylor PA, et al. Handling multiplicity in neuroimaging through bayesian lenses with multilevel modeling. *Neuroinformatics.* 2019;17(4):515-545.
42. Fjell AM, Walhovd KB, Fennema-Notestine C, et al. One-year brain atrophy evident in healthy aging. *J Neurosci.* 2009;29(48):15223-15231.
43. Crawford. LONI Image Data Archive (IDA). Accessed November 2, 2020. <https://ida.loni.usc.edu/login.jsp?project=abdc5>

SUPPORTING INFORMATION

Additional supporting information can be found online in the Supporting Information section at the end of this article.

How to cite this article: Queder N, Phelan MJ, Taylor L, et al. Joint-label fusion brain atlases for dementia research in Down syndrome. *Alzheimer's Dement.* 2022;14:e12324. <https://doi.org/10.1002/dad2.12324>